chemistry

MDPI

Article

Starting Electroosmosis in a Fibrous Porous Medium with Arbitrary Electric Double-Layer Thickness

Wei Z. Chen and Huan J. Keh *

Department of Chemical Engineering, National Taiwan University, Taipei 10617, Taiwan; r12524128@ntu.edu.tw
* Correspondence: huan@ntu.edu.tw; Tel.: +886-2-33663048

Abstract: The transient electroosmotic response in a charged porous medium consisting of a uniform array of parallel circular cylindrical fibers with arbitrary electric double layers filled with an electrolyte solution, for the stepwise application of a transverse electric field, is analyzed. The fluid momentum conservation equation is solved for each cell by using a unit cell model, where a single cylinder is surrounded by a coaxial shell of the electrolyte solution. A closed-form expression for the transient electroosmotic velocity of the bulk fluid in the Laplace transform is obtained as a function of the ratio of the cylinder radius to the Debye screening length and the porosity of the fiber matrix. The effect of the fiber matrix porosity on the continuous growth of the electroosmotic velocity over time is substantial and complicated. For a fiber matrix with larger porosity, the bulk fluid velocity takes longer to reach a certain percentage of its final value. Although the final value of the bulk fluid velocity generally increases with increasing porosity, early velocities may decrease with increasing porosity. For a given fiber matrix porosity, the transient electroosmotic velocity is a monotonically increasing function of the ratio of the cylinder radius to the Debye length.

Keywords: transient electroosmosis; circular cylinder; arbitrary electric double layer; unit cell model

check for updates

Academic Editor: Igor Alabugin

Received: 15 December 2024
Revised: 3 January 2025
Accepted: 6 January 2025
Published: 8 January 2025

Citation: Chen, W.Z.; Keh, H.J. Starting Electroosmosis in a Fibrous Porous Medium with Arbitrary Electric Double-Layer Thickness. *Chemistry* **2025**, *7*, 5. https://doi.org/10.3390/chemistry7010005

Copyright: © 2025 by the authors. Licensee MDPI, Basel, Switzerland. This article is an open access article distributed under the terms and conditions of the Creative Commons Attribution (CC BY) license (https://creativecommons.org/licenses/by/4.0/).

1. Introduction

The electroosmotic flows of electrolyte solutions in charged porous media or microchannels are of great importance in many technological areas, both fundamentally and practically. Although the elementary mathematical analysis of electroosmosis was mainly performed in the steady state [1–4], its transient behavior is sometimes as important as its steady-state behavior. In various applications, pulsating or alternating electric fields are used for electroosmotic measurements and manipulations [5–8]. Particularly, the time evolution of the fluid velocity is relevant to electroosmosis in microfluidics in the sub-millisecond range, such as biochip operations in high-speed electrokinetic separation processes, the use of short-duration pulsed electric fields to distinguish between colloidal particle velocities and background electroosmotic flow or to suppress thermal-zone broadening, and micro-pumping by means of AC or modulated DC fields [9]. The time-periodic and transient starting electroosmotic flows of electrolyte solutions in microchannels with various cross-sectional shapes have been analyzed in the past for the electric double layers of small [10,11] and arbitrary [12–14] thicknesses.

In the real applications of electroosmotic flows, a porous medium is frequently encountered. To avoid the difficulties of complex geometries, unit cell models are often used to predict the effects of interactions between small solid entities constituting the porous medium on electroosmotic velocity [15–24]. These models allow a group of entities to be

divided into numerous identical cells, each with an entity at its center. Therefore, the boundary value problem of multiple solid bodies is reduced to dealing with a single element consisting of a solid body and a concentric shell of fluid surrounding it. Different shapes of unit cells can be chosen, but a spherical or cylindrical shape is the most convenient.

The transient starting electroosmotic flow of electrolyte solutions in the axial direction of a fibrous porous medium consisting of a uniform array of parallel circular dielectric cylinders, with arbitrary electric double layer thickness and zeta potential after the application of a step-function electric field, was analyzed using a unit cell model [25]. This analysis was also extended approximately to the starting electroosmotic flow in the transverse direction of the fibrous porous medium for the case of constant zeta potential and a thin but finite double layer (say, $\kappa a \geq 10$, where κ^{-1} is the Debye screening length and a is the radius of cylinders) [26].

In the practical case of electroosmosis in charged porous media, the thickness of the electric double layers can be comparable to the pore size and the dependence of the dynamic response of the electroosmotic flow on κa over a wide range must be considered. In this paper, we present an analytical study of the transient electroosmosis induced by the sudden application of a constant transverse electric field in a matrix of parallel circular cylindrical fibers with arbitrary double-layer thickness using a unit cell model. The zeta potential (or surface charge density) of the cylinders is assumed to be uniform and small. The transient response of the electroosmotic velocity of the electrolyte solution as a function of relevant parameters is explicitly obtained.

2. Analysis

We consider a Newtonian liquid solution of arbitrary electrolytes with the viscosity η and density ρ, filled in a charged fibrous porous medium consisting of a uniform array of parallel dielectric cylinders of arbitrary radius a and Debye screening length κ^{-1} (characteristic thickness of the electric double layer). Since the initial time $t = 0$, a constant electric field E_∞ is applied in the x direction normal to the axes of the cylinders. As a result, the electrolyte solution starts flowing in the same direction with an instantaneous bulk velocity $-U(t)$ (where U is positive and negative if the cylinders are positively and negatively charged, respectively) due to electroosmosis. A unit cell model is used in which each circular cylinder is surrounded by a coaxial cylindrical shell of liquid with an outer radius b, as shown in Figure 1; therefore, the liquid-to-cell volume ratio $1 - \phi$ is equal to the porosity of the fiber matrix, where $\phi = (a/b)^2$. The origin of the polar coordinate system (r, θ) is set on the axis of the cylinder and $\theta = 0$ means the x axis. Clearly, this two-dimensional problem for a cell is symmetric about the x axis. Our goal is to determine the transient electroosmotic velocity $U(t)$.

The electrical potential distribution $\psi(r, \theta)$ in the fluid around the cylinder in a unit cell can be expressed as the equilibrium potential distribution $\psi_{eq}(r)$ induced by the surface charge of the cylinder and mobile ions in the surrounding electrical double layer (which satisfies the Poisson–Boltzmann equation) added with the perturbed potential distribution $\psi_a(r, \theta)$ caused by the external electric field E_∞ (which satisfies the Laplace equation),

$$\psi = \psi_{eq} + \psi_a, \tag{1}$$

where [22]

$$\psi_{eq} = \zeta \frac{I_1(\kappa b)K_0(\kappa r) + I_0(\kappa r)K_1(\kappa b)}{I_1(\kappa b)K_0(\kappa a) + I_0(\kappa a)K_1(\kappa b)} = \frac{\sigma}{\varepsilon\kappa} \frac{I_1(\kappa b)K_0(\kappa r) + I_0(\kappa r)K_1(\kappa b)}{I_1(\kappa b)K_1(\kappa a) - I_1(\kappa a)K_1(\kappa b)}, \tag{2}$$

$$\psi_a = -\frac{E_\infty}{\chi}\left(r + \frac{a^2}{r}\right)\cos\theta. \tag{3}$$

Here, ζ and σ are the zeta potential and surface charge density, respectively, of the cylinder, and I_n and K_n are the modified Bessel functions of order n of the first and second kinds, respectively, $\chi = 1 + \phi$ if the Dirichlet condition is used for the perturbed potential distribution on the outer boundary of the cell ($r = b$), $\chi = 1 - \phi$ if the Neumann condition is used there, and ε is the dielectric permittivity of the fluid. Note that Equation (2) is valid when the electrical potential is small (in which the Debye–Hückel approximation applies). In comparison with the Neumann condition at $r = b$, the Dirichlet condition has an advantage that both the radial and angular components of the perturbed potential gradient are specified [16,20].

The transient creeping flow of the electrolyte solution is governed by the modified Stokes equation [27]

$$\nabla^2(\nabla^2 - \frac{1}{\nu}\frac{\partial}{\partial t})\Psi = \frac{\varepsilon\kappa^2\Psi_a d\Psi_{eq}}{\eta r dr}\tan\theta, \tag{4}$$

where ν is the kinematic viscosity ($= \eta/\rho$) of the fluid, t is time, and Ψ is the Lagrange stream function. The boundary and initial conditions for the fluid velocity components v_r and v_θ in a unit cell are [24,26]

$$r = a\text{: } v_r = -\frac{1}{r}\frac{\partial\Psi}{\partial\theta} = 0,\ v_\theta = \frac{\partial\Psi}{\partial r} = 0, \tag{5}$$

$$r = b\text{: } v_r = -U\cos\theta, \tag{6a}$$

$$\tau_{r\theta} = \eta[r\frac{\partial}{\partial r}(\frac{v_\theta}{r}) + \frac{1}{r}\frac{\partial v_r}{\partial\theta}] = 0 \text{ for the Happel model,} \tag{6b}$$

$$(\nabla \times \boldsymbol{v})_z = \frac{1}{r}\frac{\partial}{\partial r}(rv_\theta) - \frac{1}{r}\frac{\partial v_r}{\partial\theta} = 0 \text{ for the Kuwabara model,} \tag{6c}$$

$$t = 0\text{: } v_r = v_\theta = 0, \tag{7}$$

where $-U(t)$ is the transient bulk fluid velocity of electroosmosis to be determined, and $U(0) = 0$. The steady-state electroosmotic velocity (as $t \to \infty$) is available in the literature [22]. For suspensions of charged spheres in electrolyte solutions, the Happel (free surface) and Kuwabara (surface with zero vorticity) models result in comparable quantities in the electrophoretic mobility. However, the Happel model has a significant advantage in that it does not require an exchange of mechanical energy between the unit cell and its surroundings [28]. Thus, the Happel model should be more satisfactory than the Kuwabara model.

In terms of the solution form $\Psi = (\varepsilon\zeta E_\infty a/\eta)g(r,t)\sin\theta$ and the Laplace transform, Equation (4) can be expressed as

$$(\frac{d^2}{dr^2} + \frac{1}{r}\frac{d}{dr} - \frac{1}{r^2})(\frac{d^2}{dr^2} + \frac{1}{r}\frac{d}{dr} - \frac{1}{r^2} - \frac{s}{\nu})\overline{g}(r) = \frac{\kappa^3}{sa}G(r), \tag{8}$$

where the transformed variable is represented by an overbar, s is the transform parameter, and

$$G(r) = \frac{1}{\chi}[1 + (\frac{a}{r})^2]\frac{I_1(\kappa b)K_1(\kappa r) - I_1(\kappa r)K_1(\kappa b)}{I_1(\kappa b)K_1(\kappa a) - I_1(\kappa a)K_1(\kappa b)}. \tag{9}$$

The general solution to Equation (4) or (8) satisfying the initial condition in Equation (7) is [27]

$$\overline{\Psi} = \frac{\varepsilon}{\eta}\zeta E_\infty a[C_1\frac{r}{a} + C_2\frac{a}{r} + C_3 I_1(Ar) + C_4 K_1(Ar) + \overline{g}_p(r)]\sin\theta, \tag{10}$$

with the particular solution

$$\overline{g}_{\mathrm{p}}(r) = \frac{-\kappa^3}{2sA^2}[\frac{r}{a}f_1(r) - \frac{a}{r}f_2(r) + 2K_1(Ar)f_3(r) - 2I_1(Ar)f_4(r)], \tag{11}$$

where

$$f_1(r) = \int_a^r G(r)\mathrm{d}r, \tag{12a}$$

$$f_2(r) = \int_a^r G(r)(\frac{r}{a})^2\mathrm{d}r, \tag{12b}$$

$$f_3(r) = \int_a^r I_1(Ar)G(r)(\frac{r}{a})\mathrm{d}r, \tag{12c}$$

$$f_4(r) = \int_a^r K_1(Ar)G(r)(\frac{r}{a})\mathrm{d}r, \tag{12d}$$

and $A = \sqrt{s/\nu}$. The coefficients C_1, C_2, C_3, and C_4 in Equation (10) result from the boundary conditions in Equations (5) and (6) as

$$C_1 = \frac{\eta\overline{U}H_1}{\varepsilon\zeta E_\infty H_0} + \frac{a\kappa^3 H_2}{A^2 s H_0}, \tag{13a}$$

$$C_2 = \frac{\eta\overline{U}H_3}{\varepsilon\zeta E_\infty H_0} + \frac{a\kappa^3 H_4}{A^2 s H_0}, \tag{13b}$$

$$C_3 = \frac{\eta\overline{U}H_5}{\varepsilon\zeta E_\infty H_0} + \frac{a\kappa^3 H_6}{A^2 s H_0}, \tag{13c}$$

$$C_4 = \frac{\eta\overline{U}H_7}{\varepsilon\zeta E_\infty H_0} + \frac{a\kappa^3 H_8}{A^2 s H_0}, \tag{13d}$$

where the nine coefficients H_0, H_1, ..., and H_8 are given in Appendix A.

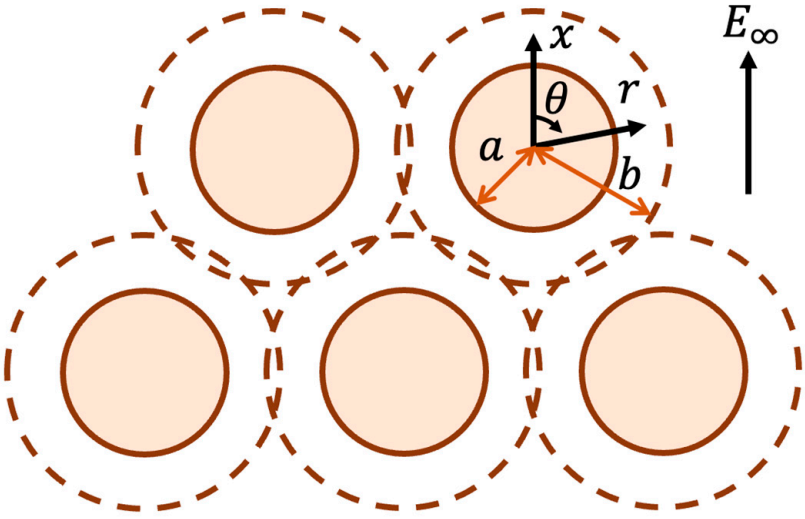


Figure 1. Geometric illustration of the unit cell model for the transient electroosmosis in an array of parallel circular cylinders.

The transformed hydrodynamic force acting on the unit cell at its virtual surface $r = b$ (in the x direction) per unit length is [27]

$$\overline{F}(s) = \int_0^{2\pi} [\eta r^3 \frac{\partial}{\partial r}(\frac{\nabla^2\overline{\Psi}}{r}) - \rho r^2 s\frac{\partial\overline{\Psi}}{\partial r} + \varepsilon\kappa^2 r\Psi_{\mathrm{eq}}\frac{\partial\Psi_{\mathrm{a}}}{s\partial\theta}]_{r=b}\sin\theta\mathrm{d}\theta. \tag{14}$$

The cell is electrically neutral as a whole (the total charge of solid plus liquid). Therefore, both the electrostatic force and the net (i.e., only hydrodynamic) force acting on it must be zero. Applying this constraint to Equation (14) (with the substitution of Equations (2), (3), (10), (11) and (13)), we obtain the normalized transient electroosmotic velocity in the Laplace transform as

$$\frac{\eta\overline{U}(s)}{\varepsilon\zeta E_\infty} = \frac{\nu\kappa^3}{2s^2}\{\frac{2(a^2+b^2)H_0}{\kappa^2 b\chi[I_1(\kappa b)K_0(\kappa a)+I_0(\kappa a)K_1(\kappa b)]} - 2ab^2H_2 + 2a^3H_4$$
$$+b^2f_1(b)H_0 + a^2f_2(b)H_0 - 2abK_1(Ab)[aH_8 - f_3(b)H_0] - 2abI_1(Ab)[aH_6 \quad (15)$$
$$+f_4(b)H_0]\}\left\{b^2H_1 - a^2H_3 + ab[I_1(Ab)H_5 + K_1(Ab)H_7]\right\}^{-1}.$$

The bulk fluid velocity can be obtained by performing the inverse Laplace transform of Equation (15) using numerical methods [29,30]. Note that the zeta potential ζ of the cylinder in Equations (10), (13) and (15) can be replaced by its surface charge density σ through their relationship given in Equation (2).

3. Results and Discussion

The normalized fluid velocity components $-\eta v_r/2\varepsilon\zeta E_\infty \cos\theta$ and $\eta v_\theta/2\varepsilon\zeta E_\infty \sin\theta$ of the transient transverse electroosmosis of an electrolyte solution around an unconfined charged circular cylinder (namely $\varphi = (a/b)^2 = 0$) in the radial and angular directions, respectively, are plotted against the scaled radial coordinate r/a in Figure 2 for several values of the scaled time $\nu t/a^2$ after the application of the electric field and the ratio of the cylinder radius to the Debye length κa. These normalized fluid velocity components around the circular cylinder in a unit cell with the solid volume fraction $\varphi = 0.04$ are also plotted against r/a in Figure 3 with the same values of $\nu t/a^2$ and κa for both the Happel and Kuwabara cell models with the Dirichlet condition of the applied electric potential distribution $\Psi_a(r,\theta)$ at the outer boundary $r = b$ of the cell ($\chi = 1+\phi$). For the given values of r/a, κa, and φ, the radial component $-\eta v_r/2\varepsilon\zeta E_\infty \cos\theta$ is always a positive increasing function of $\nu t/a^2$ to a finite constant in the steady limit $\nu t/a^2 \to \infty$ as expected (as shown in Figures 2a and 3a), while the angular component $\eta v_\theta/2\varepsilon\zeta E_\infty \sin\theta$ is a positive increasing function of $\nu t/a^2$ only at small values of r/a (locations near the cylinder surface) and may become negative and decrease with an increase in $\nu t/a^2$ at greater values of r/a (as shown in Figures 2b and 3b). For the fixed values of $\nu t/a^2$, κa, and φ, as expected, both velocity components in general increase with an increase in r/a from zero at the cylinder surface ($r/a = 1$), reach their maxima (whose locations shift toward larger r/a at a greater $\nu t/a^2$ or a smaller κa), and then decrease with a further increase in r/a (interestingly, $\eta v_\theta/2\varepsilon\zeta E_\infty \sin\theta$ may thereafter become negative and reach a minimum, whose location also shifts toward larger r/a at a greater $\nu t/a^2$ or a smaller κa, and then increase with a further increase in r/a). In the steady limit $\nu t/a^2 \to \infty$, the radial component $-\eta v_r/2\varepsilon\zeta E_\infty \cos\theta$ is a monotonically increasing function of r/a and the angular component $\eta v_\theta/2\varepsilon\zeta E_\infty \sin\theta$ is always positive. The 2D map of the electroosmotic flow field around a circular cylinder is similar to the corresponding map of the creeping flow field around a sphere, as shown in Happel and Brenner [28]. For specified values of $\nu t/a^2$, r/a, and φ, both velocity components generally increase with an increase in κa, and there are some exceptions for $\eta v_\theta/2\varepsilon\zeta E_\infty \sin\theta$. The Happel and Kuwabara cell models lead to qualitatively alike and quantitatively equivalent results of the normalized fluid velocity components (as shown in Figure 3).

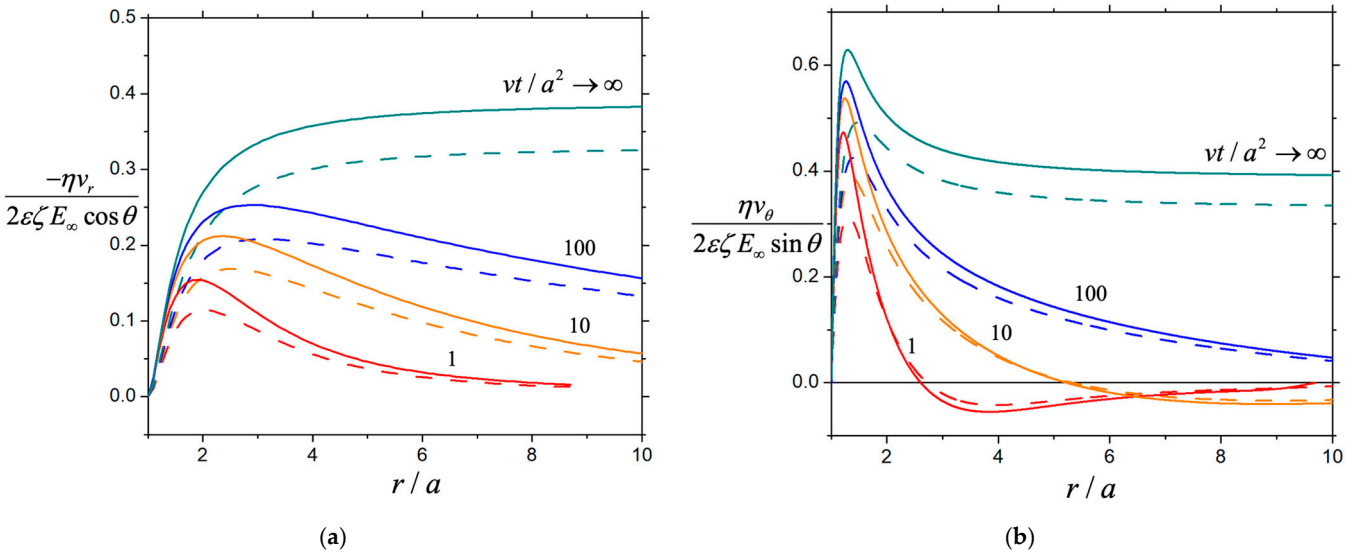


Figure 2. Normalized fluid velocity components of the transient electroosmosis around an unconfined circular cylinder ($\varphi = (a/b)^2 = 0$), versus the scaled radial coordinate r/a for various values of the scaled time $\nu t/a^2$: (**a**) $-\eta v_r/2\varepsilon\zeta E_\infty \cos\theta$; (**b**) $\eta v_\theta/2\varepsilon\zeta E_\infty \sin\theta$. The solid and dashed curves denote $\kappa a = 10$ and $\kappa a = 5$, respectively.

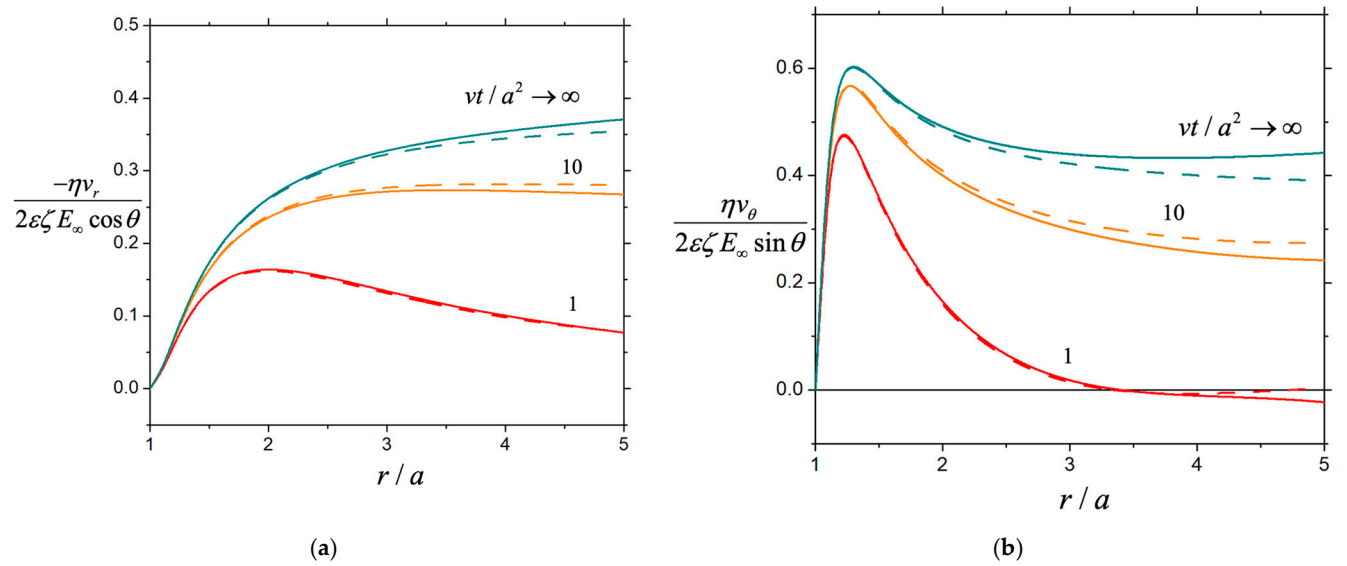


Figure 3. Normalized fluid velocity components of the transient electroosmosis around the circular cylinder in a unit cell with $\varphi = (a/b)^2 = 0.04$ and $\kappa a = 10$ versus the scaled radial coordinate r/a for the various values of the scaled time $\nu t/a^2$: (**a**) $-\eta v_r/2\varepsilon\zeta E_\infty \cos\theta$; (**b**) $\eta v_\theta/2\varepsilon\zeta E_\infty \sin\theta$. The solid and dashed curves denote the Happel and Kuwabara cell models, respectively.

The normalized fluid velocity $\eta U/\varepsilon\zeta E_\infty$ of the bulk electrolyte solution undergoing transient transverse electroosmosis in a fibrous porous medium is plotted against the scaled time $\nu t/a^2$ and fiber volume fraction ϕ in Figures 4 and 5, respectively, for the different values of the ratio of the cylinder radius to the Debye length κa for both the Happel and Kuwabara cell models with the Dirichlet condition ($\chi = 1 + \phi$). It is understood that $\eta U/\varepsilon\zeta E_\infty$ equals unity in the limiting case of $\nu t/a^2 \to \infty$, $\varphi = 0$, and $\kappa a \to \infty$ [26]. The effect of ϕ on the continuous growth of the electroosmotic velocity with time is substantial and complicated, and a greater $\nu t/a^2$ is needed for $\eta U/\varepsilon\zeta E_\infty$ to attain a definite percentage of its terminal value (as $\nu t/a^2 \to \infty$) for a fiber matrix with a greater porosity (smaller ϕ). For a given value of κa, this terminal value generally increases with a decrease in

ϕ (an increase in the porosity) as expected [22], while $\eta U/\varepsilon\zeta E_\infty$ at an early time may decrease with a decrease in ϕ, since the characteristic time of the transient electroosmosis is greater and the fluid velocity of the bulk electrolyte solution at the outer edge of the unit cell is hardly influenced by the transient electroosmosis starting from near the charged surface of the fiber cylinder for the porous medium with a smaller ϕ. The Happel model in general results in a greater value of the normalized bulk fluid velocity than the Kuwabara model does, but there are exceptions (qualitatively different terminal velocities may be obtained from them, as shown for a thicker double layer and a small solid volume fraction in Figure 5a). Since the Happel model has a significant advantage in that it does not require an exchange of mechanical energy between the unit cell and the environment, the Happel model should be more accurate than the Kuwabara model.

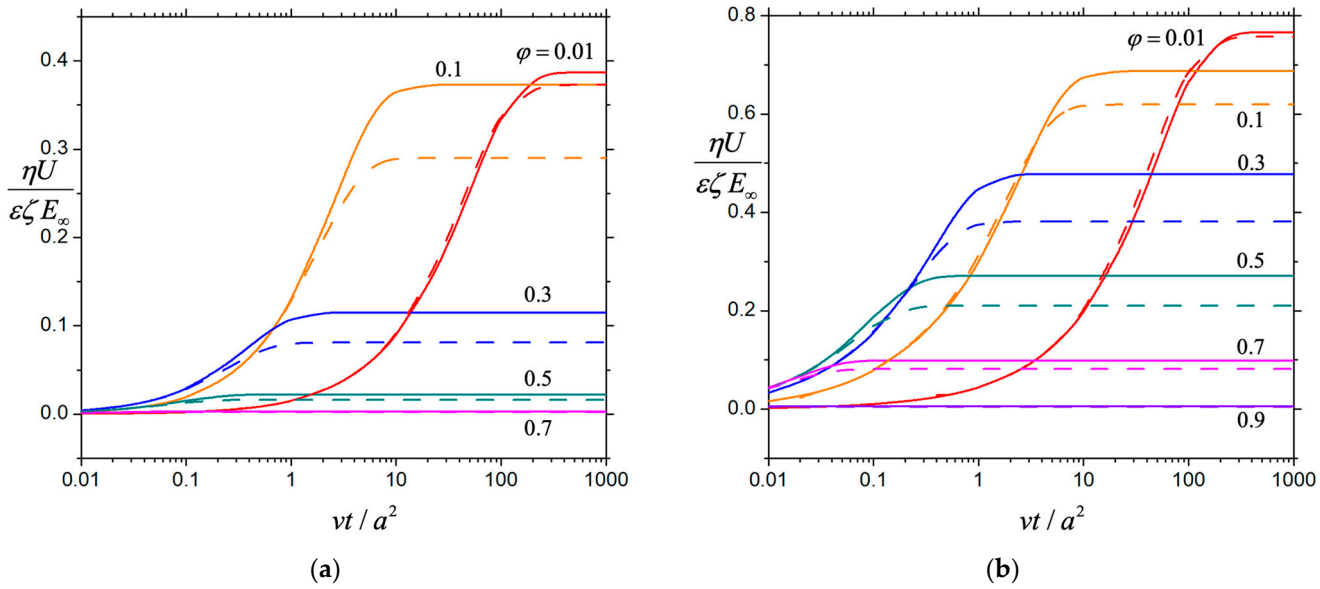


Figure 4. Normalized bulk fluid velocity $\eta U/\varepsilon\zeta E_\infty$ of the transient electroosmosis in a fibrous porous medium versus the scaled time $\nu t/a^2$ for various values of the solid volume fraction ϕ: (**a**) $\kappa a = 1$; (**b**) $\kappa a = 10$. The solid and dashed curves denote the Happel and Kuwabara cell models, respectively.

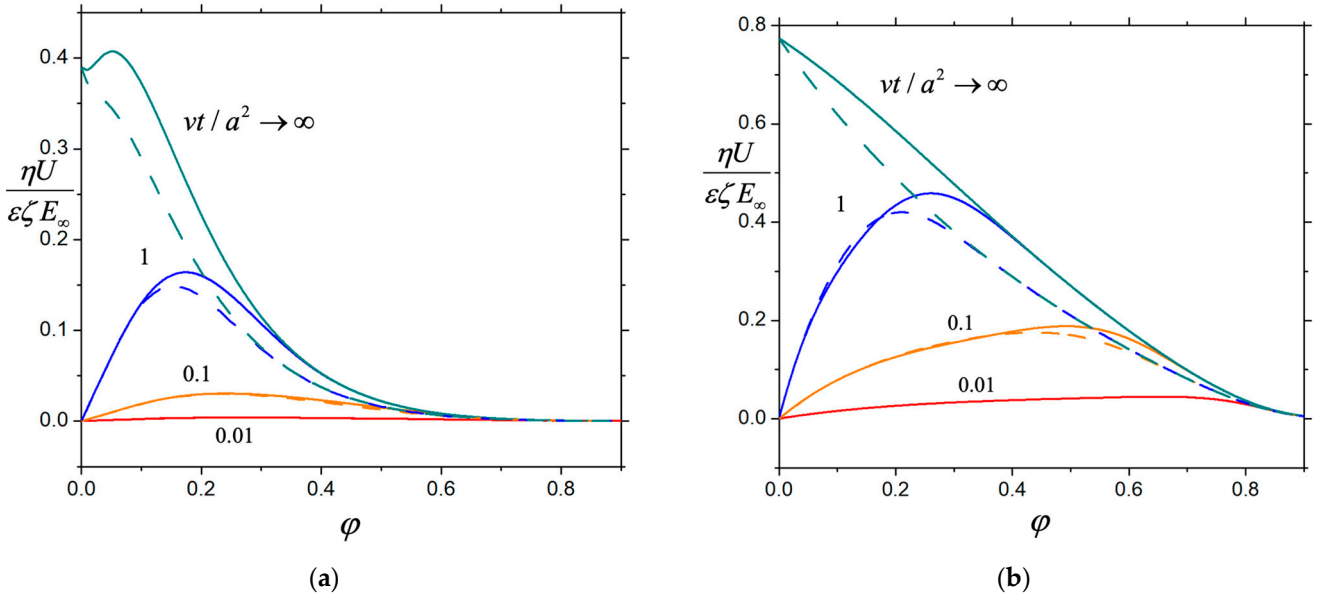


Figure 5. Normalized bulk fluid velocity $\eta U/\varepsilon\zeta E_\infty$ of the transient electroosmosis in a fibrous porous medium versus the solid volume fraction ϕ for various values of the scaled time $\nu t/a^2$: (**a**) $\kappa a = 1$; (**b**) $\kappa a = 10$. The solid and dashed curves denote the Happel and Kuwabara cell models, respectively.

In Figure 6, the normalized transient electroosmotic velocity $\eta U/\varepsilon\zeta E_\infty$ of the bulk electrolyte solution in a fibrous porous medium with $\phi = 0.25$ is plotted against the scaled time $\nu t/a^2$ and ratio of the cylinder radius to the Debye length κa. Again, $\eta U/\varepsilon\zeta E_\infty$ grows incessantly with $\nu t/a^2$ for a given value of κa. For fixed values of $\nu t/a^2$ and ϕ, this velocity is a monotonically increasing function of κa. In comparison with our results in Figures 4–6 for an arbitrary value of κa, the calculations in the thin-double-layer approximation to the starting electroosmosis in the fibrous porous medium with $\kappa a \geq 10$ [26] overestimates the electroosmotic velocity of the fluid with the same value of κa.

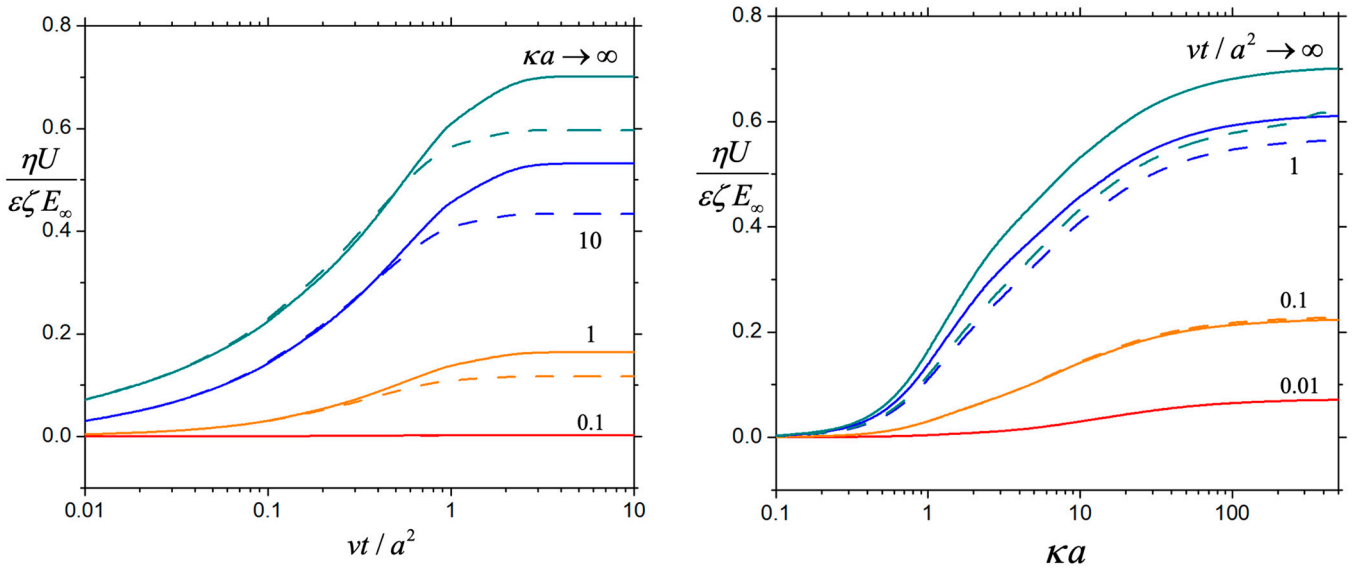


Figure 6. Normalized bulk fluid velocity $\eta U/\varepsilon\zeta E_\infty$ of the transient electroosmosis in a fibrous porous medium with the solid volume fraction $\phi = 0.25$: (**a**) versus $\nu t/a^2$ for various values of κa; (**b**) versus κa for various values of $\nu t/a^2$. The solid and dashed curves denote the Happel and Kuwabara cell models, respectively.

4. Concluding Remarks

In this paper, the start-up of the electroosmosis of electrolyte solutions upon the stepwise application of an electric field transversely to a charged fibrous porous medium consisting of parallel circular cylinders with arbitrary electric double layers is analytically investigated. The fluid momentum equation is solved by using both the Happel and Kuwabara unit cell models. A closed-form expression for the transient electroosmotic velocity of the bulk fluid $\eta U/\varepsilon\zeta E_\infty$ in the Laplace transform is obtained as a function of the scaled elapsed time $\nu t/a^2$, ratio of the cylinder radius to the Debye screening length κa, and the porosity of the fiber matrix $1 - \phi$. The effect of φ on the continuous growth of $\eta U/\varepsilon\zeta E_\infty$ over time is substantial and complex. For a fiber matrix with smaller φ (larger porosity), $\eta U/\varepsilon\zeta E_\infty$ takes longer to reach a certain percentage of its final value. Although the final value of $\eta U/\varepsilon\zeta E_\infty$ generally decreases with increasing φ, early velocities may increase with increasing φ. For a given φ, the transient electroosmotic velocity is a monotonically increasing function of the ratio of κa.

The starting electroosmosis of electrolyte solutions in the axial direction of the fibrous porous medium composed of parallel circular cylinders was examined by using the unit cell model and an analytical solution of the electroosmotic velocity was obtained for arbitrary κa, ϕ, and $\nu t/a^2$ [25]. For the general problem of transient electroosmosis in the fibrous medium caused by an external electric field in an arbitrary direction with respect to the axes of its constitutive cylinders, the solution of the electroosmotic velocity can be obtained

by the vectorial addition of the previous result for the axial flow and the present result for the transverse flow due to the linearity.

In a real system, there should be a slab of fibrous material between two reservoirs and a voltage should be applied. Some entrance effect may be considered in our calculations for such a realistic case to show how large the electroosmotic flow may be and to provide some ideas on how the entrance effect may enter in the problem, like in the case of other electrokinetic phenomena [31–33].

Author Contributions: Conceptualization, H.J.K.; methodology, H.J.K. and W.Z.C.; investigation, H.J.K. and W.Z.C.; writing—original draft preparation, H.J.K. and W.Z.C.; writing—review and editing, H.J.K.; supervision, H.J.K.; funding acquisition, H.J.K. All authors have read and agreed to the published version of the manuscript.

Funding: This research was funded by the National Science and Technology Council, Taiwan (Republic of China) grant number MOST 110-2221-E-002-017-MY3.

Data Availability Statement: Data are contained within the article.

Conflicts of Interest: The authors declare no conflicts of interest. The funders had no role in the design of the study; in the collection, analyses, or interpretation of data; in the writing of the manuscript; or in the decision to publish the results.

Appendix A

The coefficients H_0, H_1, ..., and H_8 in Equation (13) are given as follows:

$$H_0 = 8 - 2AI_0(Ab)[A(a^2-b^2)K_0(Aa) + 2aK_1(Aa)] + AbI_1(Ab)[dK_0(Aa) + 2AaK_1(Aa)]$$
$$-A\Big\{2aI_1(Aa)R - I_0(Aa)[2A(a^2-b^2)K_0(Ab) + bdK_1(Ab)]\Big\},$$
$$H_1 = 4 + Ab\{MK_0(Aa) - I_0(Aa)[2AbK_0(Ab) + NK_1(Ab)]\},$$
$$H_2 = (2a)^{-1}\{f_1(b)H_1 + Aa[f_2(b)Aa\{AbI_1(Ab)K_0(Aa) - 2I_0(Ab)K_0(Aa) + I_0(Aa)R\} + 2f_3(b)Q + 2f_4(b)P]\},$$
$$H_3 = b\Big\{Aa[bMK_1(Aa) + bNI_1(Aa) - 2a]K_2(Aa) - N\Big(b - Aa^2T\Big)\Big\}\{a[aK_1(Ab) - bK_1(Aa)]\}^{-1},$$
$$H_4 = [16\Big\{bK_1(Aa) - aK_1(Ab)\}\Big(b - Aa^2T\Big)\{2af_2(b) - bf_3(b)N - bf_4(b)M\}$$
$$+8N(b - Aa^2T)\Big\{a[af_2(b) - 2bf_3(b)K_1(Ab) + 2bf_4(b)I_1(Ab)] - b^2f_1(b)\Big\}$$
$$+8AaK_2(Aa)\{bMK_1(Aa) + bNI_1(Aa) - 2a\}\Big\{b^2f_1(b) - a[af_2(b) - 2bf_3(b)K_1(Ab)$$
$$+2bf_4(b)I_1(Ab)]\}]\Big\{16a^2b[aK_1(Ab) - bK_1(Aa)]\Big\}^{-1},$$
$$H_5 = 2a^{-1}[bN - 2Aa^2K_2(Aa)],$$
$$H_6 = a^{-1}\Big[f_1(b)H_5/2 + Aaf_2(b)Q + Af_3(b)\Big\{2aK_1(Aa)R + K_0(Aa)[2A(a^2-b^2)K_0(Ab) + bdK_1(Ab)]\Big\}$$
$$+f_4(b)\Big\{2AI_0(Ab)[A(a^2-b^2)K_0(Aa) + 2aK_1(Aa)] + AbI_1(Ab)[dK_0(Aa) - 2AaK_1(Aa)] - 4\Big\}],$$
$$H_7 = 2a^{-1}[bM - 2Aa^2I_2(Aa)],$$
$$H_8 = a^{-1}\Big[f_1(b)H_7/2 + f_2(b)AaP + f_3(b)\Big\{4 - 2aAI_1(Aa)R + AI_0(Aa)[2A(a^2-b^2)K_0(Ab) - bdK_1(Ab)]\Big\}$$
$$+Af_4(b)\Big\{2aI_1(Aa)[-2I_0(Ab) + AbI_1(Ab)] + I_0(Aa)[2A(a^2-b^2)I_0(Ab) + bdI_1(Ab)]\Big\}],$$

for the Happel model, and

$$H_0 = a^{-1}\Big\{I_1(Ab)[A(a^2-b^2)K_0(Aa) + 2aK_1(Aa)] + K_1(Ab)[A(a^2-b^2)I_0(Aa) - 2aI_1(Aa)]\Big\},$$

$$H_1 = -Aa^{-1}b^2[I_1(Ab)K_0(Aa) + I_0(Aa)K_1(Ab)],$$

$$H_2 = (2a^2)^{-1}\Big\{AI_0(Aa)K_1(Ab)[-b^2f_1(b) + a^2f_2(b)] - 2aK_1(Ab)f_3(b)$$

$$+I_1(Ab)[AK_0(Aa)\Big\{a^2f_2(b) - b^2f_1(b)\Big\} + 2af_4(b)]\},$$

$$H_3 = Aa^{-1}b^2T,$$

$$H_4 = (2a^3)^{-1}\Big\{Aa[b^2f_1(b) - a^2f_2(b)]T + 2b^2f_3(b)K_1(Ab) - 2b^2f_4(b)I_1(Ab)\Big\},$$

$$H_5 = 2a^{-2}b^2K_1(Ab),$$

$$H_6 = a^{-3}\Big\{b^2f_1(b)K_1(Ab) + a[\Big\{A(a^2 - b^2)K_0(Aa) + 2aK_1(Aa)\Big\}\{f_3(b)K_1(Ab) - f_4(b)I_1(Ab)\} - af_2(b)K_1(Ab)]\Big\},$$

$$H_7 = -2a^{-2}b^2I_1(Ab),$$

$$H_8 = a^{-3}\Big\{a[af_2(b)I_1(Ab) + \Big\{A(a^2 - b^2)I_0(Aa) - 2aI_1(Aa)\Big\}\{f_3(b)K_1(Ab) - f_4(b)I_1(Ab)\}] - b^2f_1(b)I_1(Ab)\Big\},$$

for the Kuwabara model, where

$$M = 2AbI_0(Ab) + (4 + A^2b^2)I_1(Ab),$$

$$N = 2AbK_0(Ab) + (4 + A^2b^2)K_1(Ab),$$

$$P = 2I_0(Aa) - 2I_0(Ab) + AbI_1(Ab),$$

$$Q = 2K_0(Aa) - 2K_0(Ab) - AbK_1(Ab),$$

$$R = 2K_0(Ab) + AbK_1(Ab),$$

$$T = I_2(Aa)K_1(Ab) + I_1(Ab)K_2(Aa),$$

$$d = A^2(a^2 - b^2) - 4$$

References

1. Rice, C.L.; Whitehead, R. Electrokinetic flow in a narrow cylindrical capillary. *J. Phys. Chem.* **1965**, *69*, 4017–4024. [CrossRef]
2. Squires, T.M.; Bazant, M.Z. Induced-charge electro-osmosis. *J. Fluid Mech.* **2004**, *509*, 217–252. [CrossRef]
3. Mao, M.; Sherwood, J.D.; Ghosal, S. Electro-osmotic flow through a nanopore. *J. Fluid Mech.* **2014**, *749*, 167–183. [CrossRef]
4. Di Muccio, G.; della Rocca, B.M.; Chinappi, M. Geometrically induced selectivity and unidirectional electroosmosis in uncharged nanopores. *ACS Nano* **2022**, *16*, 8716–8728. [CrossRef] [PubMed]
5. Hu, Z.; Zhao, T.; Wang, H.; Zhao, W.; Wang, K.; Bai, J.; Wang, G. Asymmetric temporal variation of oscillating AC electroosmosis with a steady pressure-driven flow. *Exp. Fluids* **2020**, *61*, 233. [CrossRef]
6. Ding, H.; Zhong, X.; Liu, B.; Shi, L.; Zhou, T.; Zhu, Y. Mixing mechanism of a straight channel micromixer based on light-actuated oscillating electroosmosis in low-frequency sinusoidal AC electric field. *Microfluid. Nanofluid.* **2021**, *25*, 26. [CrossRef]
7. Yu, Y.; Li, J.-C.; Lin, H.; Li, K.; Yi, F. Study on ethanol driven by alternating current electroosmosis in microchannels. *Sens. Actuators A Phys.* **2023**, *351*, 114174. [CrossRef]
8. Dutta, D.; Smith, K.; Palmer, X. Long-range ACEO phenomena in microfluidic channel. *Surfaces* **2023**, *6*, 145–163. [CrossRef]
9. Yossifon, G.; Frankel, I.; Miloh, T. Macro-scale description of transient electro-kinetic phenomena over polarizable dielectric solids. *J. Fluid Mech.* **2009**, *620*, 241–262. [CrossRef]
10. Hanna, W.T.; Osterle, J.F. Transient electro-osmosis in capillary tubes. *J. Chem. Phys.* **1968**, *49*, 4062–4068. [CrossRef]
11. Deng, S.; Xiao, T. Transient two-layer electroosmotic flow and heat transfer of power-law nanofluids in a microchannel. *Micromachines* **2022**, *13*, 405. [CrossRef]
12. Keh, H.J.; Tseng, H.C. Transient electrokinetic flow in fine capillaries. *J. Colloid Interface Sci.* **2001**, *24*, 450–459. [CrossRef]
13. Jian, Y.; Yang, L.; Liu, Q. Time periodic electro-osmotic flows through a microannulus. *Phys. Fluids* **2010**, *22*, 042001. [CrossRef]
14. Sin, J.-S.; Ri, N.-I.; Kim, H.-C.; Hyon, S.-H. Impact of charged soft layers on electroosmosis of Maxwell fluids in soft nanochannels. *Phys. Fluids* **2023**, *35*, 112002. [CrossRef]
15. Levine, S.; Neale, G.H. The prediction of electrokinetic phenomena within multiparticle systems I. Electrophoresis and electroosmosis. *J. Colloid Interface Sci.* **1974**, *47*, 520–529. [CrossRef]

16. Zharkikh, N.I.; Shilov, V.N. Theory of collective electrophoresis of spherical particles in the Henry approximation. *Colloid J. USSR Engl. Transl.* **1982**, *43*, 865–870.
17. Kozak, M.W.; Davis, E.J. Electrokinetic phenomena in fibrous porous media. *J. Colloid Interface Sci.* **1986**, *112*, 403–411. [CrossRef]
18. Ohshima, H. Electroosmotic velocity in fibrous porous media. *J. Colloid Interface Sci.* **1999**, *210*, 397–399. [CrossRef]
19. Keh, H.J.; Wei, Y.K. Diffusioosmosis and electroosmosis of electrolyte solutions in fibrous porous media. *J. Colloid Interface Sci.* **2002**, *252*, 354–364. [CrossRef]
20. Zholkovskiy, E.K.; Masliyah, J.H.; Shilov, V.N.; Bhattacharjee, S. Electrokinetic phenomena in concentrated disperse systems: General problem formulation and spherical cell approach. *Adv. Colloid Interface Sci.* **2007**, *134–135*, 279–321. [CrossRef] [PubMed]
21. Ahualli, S.; Jimenez, M.L.; Carrique, F.; Delgado, A.V. AC electrokinetics of concentrated suspensions of soft particles. *Langmuir* **2009**, *25*, 1986–1997. [CrossRef] [PubMed]
22. Keh, H.J.; Wu, Y.Y. Electroosmotic velocity and electric conductivity in a fibrous porous medium in the transverse direction. *J. Phys. Chem. B* **2011**, *115*, 9168–9178. [CrossRef]
23. Su, Y.W.; Keh, H.J. Electrokinetic flow of salt-free solutions in a fibrous porous medium. *J. Phys. Chem. B* **2019**, *123*, 9724–9730. [CrossRef]
24. Chen, W.L.; Keh, H.J. Electroosmosis and electric conduction of electrolyte solutions in charge-regulating fibrous porous media. *Colloids Interfaces* **2021**, *5*, 19. [CrossRef]
25. Chen, G.Y.; Keh, H.J. Start-up of electrokinetic flow in a fibrous porous medium. *J. Phys. Chem. C* **2014**, *118*, 2826–2833. [CrossRef]
26. Chiang, C.C.; Keh, H.J. Transient electroosmosis in the transverse direction of a fibrous porous medium. *Colloids Surf. A* **2015**, *481*, 577–582. [CrossRef]
27. Li, M.X.; Keh, H.J. Start-up electrophoresis of a cylindrical particle with arbitrary double layer thickness. *J. Phys. Chem. B* **2020**, *124*, 9967–9973. [CrossRef] [PubMed]
28. Happel, J.; Brenner, H. *Low Reynolds Number Hydrodynamics*; Nijhoff: Dordrecht, The Netherlands, 1983.
29. Talbot, A. The accurate numerical inversion of Laplace transforms. *IMA J. Appl. Math.* **1979**, *23*, 97–120. [CrossRef]
30. Murli, A.; Rizzardi, M. Talbot's method for the Laplace inversion problem. *ACM Trans. Math. Softw.* **1990**, *16*, 158–168. [CrossRef]
31. Gadaleta, A.; Sempere, C.; Gravelle, S.; Siria, A.; Fulcrand, R.; Ybert, C.; Bocquet, L. Sub-additive ionic transport across arrays of solid-state nanopores. *Phys. Fluids* **2014**, *26*, 012005. [CrossRef]
32. Yaroshchuk, A.; Bondarenko, M.P. Interaction of potential sources in infinite 2D arrays: Diffusion through composite membranes, micro-electrochemistry, entrance resistance, and other examples. *Adv. Theory Simul.* **2021**, *4*, 2100128. [CrossRef]
33. Baldelli, M.; Di Muccio, G.; Viola, F.; Giacomello, A.; Cecconi, F.; Balme, S.; Chinappi, M. Performance of single nanopore and multi-pore membranes for blue energy. *ChemPhysChem* **2024**, *25*, e202400395. [CrossRef]

Disclaimer/Publisher's Note: The statements, opinions and data contained in all publications are solely those of the individual author(s) and contributor(s) and not of MDPI and/or the editor(s). MDPI and/or the editor(s) disclaim responsibility for any injury to people or property resulting from any ideas, methods, instructions or products referred to in the content.